Properties of metal–water interfaces studied from first principles

2009 New J. Phys. 11 125003

(http://iopscience.iop.org/1367-2630/11/12/125003)

New Journal of Physics
The open-access journal for physics

Properties of metal–water interfaces studied from first principles

Sebastian Schnur and Axel Groß
Institut für Theoretische Chemie, Universität Ulm, D-89069 Ulm, Germany
E-mail: axel.gross@uni-ulm-de

New Journal of Physics **11** (2009) 125003 (25pp)
Received 2 April 2009
Published 11 December 2009
Online at http://www.njp.org/
doi:10.1088/1367-2630/11/12/125003

Abstract. Properties of the metal–water interface have been addressed by periodic density functional theory calculations, in particular with respect to the electronic and geometric structures of water bilayers on several transition metal surfaces. It will be demonstrated that the presence of the metal substrate leads to a significant polarization of the water bilayer. This causes a substantial water-induced reduction of the work function in spite of the weak water–metal interaction, but it is not associated with a significant change of the electronic structure of the metal substrates. The structure and the vibrational spectra of water bilayers at room temperatures have been studied performing *ab initio* molecular dynamics simulations. The simulations suggest that the water bilayer structure on noble metals is not stable at room temperature, whereas on more strongly interacting metal surfaces some ordering of the water layer persists. In addition, metal–water interfaces under electrochemical conditions, i.e. for charged metal substrates, are addressed. Our simulations show that the charging of the surface leads to characteristic changes in the wall–oxygen distribution and the vibrational spectra.

Contents

1. Introduction

The water–metal interface is of significant interest not only from a fundamental but also from an applied point of view in the context of corrosion and catalysis. This is particularly true in electrochemistry that has attracted a lot of attraction recently due to its relevance for hydrogen production and energy storage and conversion, as realized, e.g. in fuel cells. This importance has motivated a huge number of experimental [1]–[3] and theoretical [4]–[9] surface science studies as well as more electrochemically oriented research efforts [10, 11].

In spite of the numerous studies, there is still a rather large number of questions left open. For example, it is not clear whether at room temperature the water at a metal surface has a crystalline ice-like structure or whether it is liquid-like. On late transition metal surfaces, in particular with hexagonal symmetry, it has been traditionally assumed that water adsorbs in a bilayer structure [9] whose structure is similar to that of the densest layer of ice [1]. In this structure, every second water molecule is oriented parallel to the surface bound with its oxygen atom to a top site of the metal surface. For the other water molecules, there are in fact two different possible orientations, namely the so-called H-down and H-up structures with one hydrogen atom either pointing toward or away from the surface. Typically, the adsorption energies of both types of bilayers are similar. However, on the less noble metals Ru, Rh and Ni that exhibit a stronger interaction with the water molecules, a half-dissociated overlayer is more stable [8, 9, 12] in which every second water molecule is dissociated to OH.

While it is of course important to determine the energetically most stable structure of water bilayers on metal substrates, in most applications the metal–water interface under ambient conditions is of interest, i.e. at temperatures around room temperature. There have been numerous molecular dynamics studies addressing the structure of the metal–water interface at finite temperatures using parameterized interaction potentials [13]–[16]. While classical potentials might reproduce structural properties of the water quite satisfactorily [17]–[19], the interaction between the metal and the water molecules is usually not described reliably due to the inability to reproduce many-body effects in the metal–molecule interaction. This situation can be significantly improved by *ab initio* molecular dynamics (AIMD) simulations, in which the forces necessary to integrate the classical equations of motion are determined 'on the fly' by first-principles electronic structure calculations, in particular based on density functional theory (DFT). Although there are still concerns with respect to the adequacy of current DFT functionals [20], DFT calculations correspond to an electronic structure methodology that

combines numerical efficiency with sufficient accuracy. Recently there have been first AIMD studies addressing the metal–water interface [4]–[7], but because of the high computational effort these simulations were restricted to rather short simulation times or small unit cells that limited the validity of the conclusions. Yet, the ever-increasing computer power allows us to extend the parameters of the AIMD simulations to conditions that allow statistically more relevant conclusions.

A further complication for the theoretical treatment of the water–metal interface arises from the fact that in electrochemistry where these interfaces are of particular importance the electrode potential is varied leading to charged surfaces. In fact, there have already been several attempts to model external fields or varying electrode potentials at the solid–liquid interface within periodic DFT calculations [21]–[27]. These studies provided valuable insights into fundamental processes at the electrochemical solid–liquid interface. There has already been an AIMD study addressing the structure of water under acidic conditions for different electrode potentials [28, 29]. Still there is no commonly accepted method to describe varying electrode potentials in periodic DFT calculations.

Recently, it has been noted that the presence of a water bilayer on a close-packed metal surface hardly influences the electronic structure of the metal due to the weak interaction between the metal and water [30]. At the same time, the presence of water changes the work function of metal electrodes quite significantly [31]. It is not surprising that the effect of H-down and H-up water bilayers on the work function of metal surfaces depends strongly on the type of the bilayer because of the opposite sign of their dipole moment normal to the surface. The differences in the work function change induced by the two types of bilayers can be more than 2 eV, and it has already been pointed out that this large difference might lead to a charge control of the water monolayer/metal interface, i.e. the stable water bilayer structure can be tuned by changing the surface charge [31]. However, it is quite surprising that on Pd(111) both types of bilayers lower the work function in spite of the small influence on the electronic structure of the metal [31]. The reason for this phenomenon, however, has to the best of our knowledge not yet been addressed. Furthermore, it is still debated how ambient conditions influence the geometric and electronic structures of metal–water interfaces.

In this paper, we focus on structural and electronic properties of the first layer of water on metal–water interfaces. We will first briefly review the current understanding of the structure of the water–metal interface based on first-principles studies. We concentrate on close-packed metal surfaces and on hexagonal ice-like bilayer structures that have been experimentally identified as the prevailing structures of water on these close-packed surfaces [1, 2]. We will then address the surprising change of the work function upon the adsorption of water bilayers in particular focusing on the polarization of the water bilayers on Au(111), Ag(111), Pt(111), Pd/Au(111) and Ru(0001). The Pd/Au(111) overlayer system that consists of a Pd monolayer deposited pseudomorphically on Au(111) has been chosen since it interacts with water almost as strongly as Pt(111) [22], but has a lattice constant that is larger by 5%. Next we present AIMD studies of water layers on these metal substrates addressing the question of whether the hexagonal ice-like water bilayers are stable at room temperature. Finally, after discussing different approaches to include varying electrode potentials in DFT calculations, we will estimate the effect of external electric fields on the stability of the water bilayer by using charged electrodes in the AIMD simulations.

2. Computational details

All calculations were carried out using the periodic DFT package VASP [32], employing the generalized gradient approximation (GGA) to describe the exchange–correlation effects within the exchange–correlation functional by Perdew, Burke and Ernzerhof (PBE) [33]. It has been shown that this functional gives a reasonable description of the properties of water [20, 34, 35]. The ionic cores were represented by projector augmented wave (PAW) potentials [36] as constructed by Kresse and Joubert [37]. The electronic one-particle wave function were expanded in a plane-wave basis set up to an energy cutoff of 400 eV. The metal substrates were represented by four-layer slabs.

The energy minimum structures of the water bilayers were determined within a $\sqrt{3} \times \sqrt{3}R30^\circ$ surface unit cell using $9 \times 9 \times 1$ k-points until the energies were converged to within 10^{-4} eV. AIMD simulations were performed using the Verlet algorithm with a time step of 1 fs at a temperature of 300 K within the microcanonical ensemble in a larger $2\sqrt{3} \times 2\sqrt{3}R30^\circ$ unit cell to reduce the constraints on the lateral geometry of the water structures. A second water layer was placed on top of the first one in order to model a surrounding water environment. To prevent desorption of this second, weakly bound water layer, the height of two oxygen atoms of the eight water molecules of the second layer in the unit cell was fixed. The AIMD runs were started with an initial ideal bilayer configuration and random velocities. The first 1 ps we considered as the thermalization period. For the AIMD simulations, the energy cutoff was reduced to 350 eV and $2 \times 2 \times 1$ k-points were used to get a compromise between sufficient accuracy and manageable simulation time. The total energy in the AIMD runs was typically conserved within 50 meV for the long runs extending to more than 10 ps.

3. Structure of water bilayers on transition metal surfaces

In general, the interaction of water molecules with metal surfaces is relatively weak. According to DFT calculations, the adsorption energies for single water molecules on (111) metal surfaces range from -0.1 to -0.4 eV with the binding strength ordered according to Au < Ag < Cu < Pd < Pt < Ru < Rh [9] for some typical late transition metals. Single water molecules bind to metal surfaces via their oxygen atom at top sites at distances between 2.25 Å (Cu) and 3.02 Å (Au) from the uppermost metal layer which is much larger than typical distances of chemisorbed species.

As far as water layers on metal surfaces are concerned, it has been traditionally assumed that they form an ice-like hexagonal bilayer structure. In this structure, every second water molecule is bound via the oxygen atom to the metal in a parallel fashion similar to the adsorption configuration of the water monomer. The remaining water molecules can be oriented in two different fashions, namely with one hydrogen atom pointing either toward or away from this surface. These so-called H-down and H-up structures are illustrated in figure 1(a) and (b), respectively. Energetically, these layers are very similar on close-packed transition metals within 0.05 eV per water molecule [8, 9]. This can be seen in our calculated values of the water adsorption energies on the considered surfaces listed in table 1 where the adsorption energies, as elsewhere in the paper, are given per water molecule with respect to the free water molecule in the gas phase. Our results are close to previously published ones [7]–[9], [38]. Note that the remaining small discrepancies are due to the different treatment of the ionic cores. In all cases considered by us, the H-down bilayer is slightly more than or equally stable as the H-up bilayer,

Table 1. Adsorption energies of the H-up and the H-down water bilayers on Au(111), Ag(111), Pt(111), Pd/Au(111) and Ru(0001) in eV per water molecule with respect to the free water molecule.

E_a (eV)	Au(111)	Ag(111)	Pt(111)	Pd/Au(111)	Ru(0001)
H-up	−0.41	−0.41	−0.45	−0.44	−0.49
H-down	−0.43	−0.43	−0.48	−0.48	−0.49

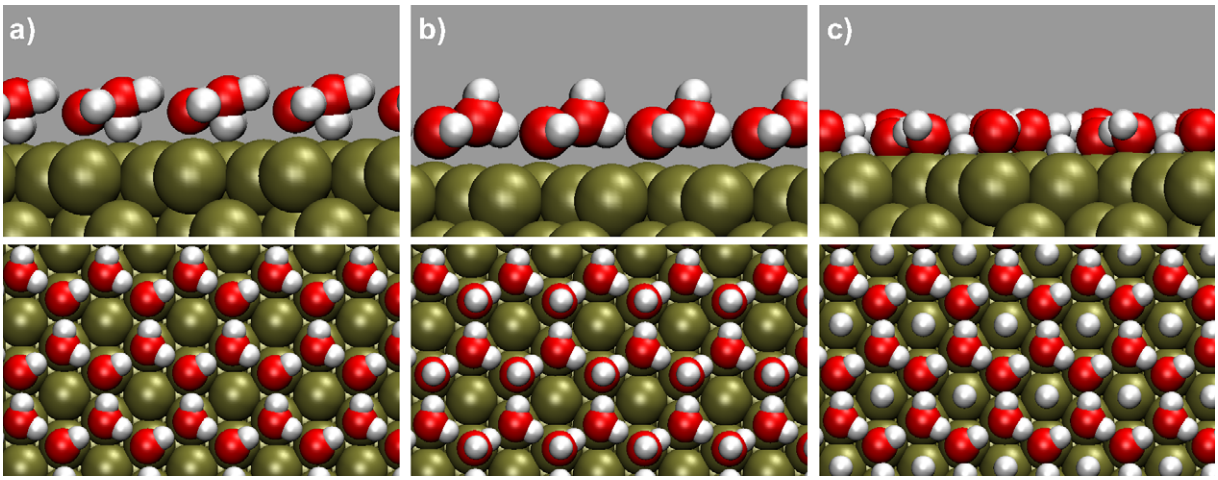

Figure 1. Side and top view of the water bilayer structures: (a) H-down bilayer, (b) H-up water bilayer, (c) half dissociated water-OH-bilayer with the additional hydrogen atoms at the center of the hexagonal rings.

but in fact on Ni(111) and Cu(111) the H-up geometry is favored [8, 9]. It is also important to realize that the largest fraction of the energy gain upon the water bilayer formation on the metal substrates stems from the water–water interaction with only a minor portion of about 20–30% being due to the water–metal interaction [9].

However, for metals such as Ru, Rh or Ni that interact more strongly with water, the water bilayers are energetically not stable with respect to dissociation. According to DFT calculations [9], they instead form a half-dissociated overlayer with every second water molecule dissociated to OH (see figure 1(c)), as first suggested for water on Ru(0001) [12, 39]. We also find that on Ru(0001) the half-dissociated water layer ($E_a = 0.71$ eV, assuming that the additional hydrogen atoms are located at the center of the hexagonal rings, as depicted in figure 1(c)) is significantly more stable than the bilayer structures. It is, however, still debated whether the half-dissociated water bilayer indeed is formed since its formation might be hindered by large barriers [39, 40].

Of particular importance is the Pt–water interface since Pt is an important electrode material, for example, in fuel cells. On Pt, the water bilayer should still stay intact. It was recently shown that the electronic structure of the Pt surfaces is hardly influenced by the presence of water [30] because of the weak water–metal interaction. As a consequence, adsorption energies of chemisorbed species are not significantly altered by the presence of a water bilayer [22].

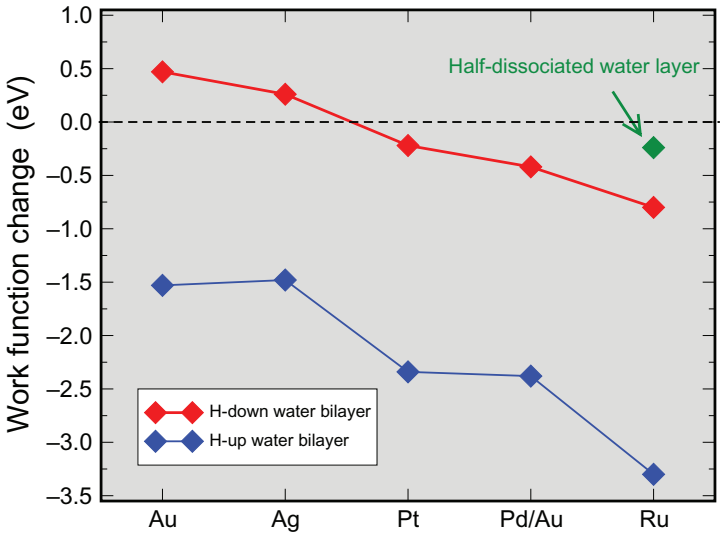

Figure 2. Calculated work function change induced by the presence of H-up and H-down water bilayers on Au(111), Ag(111), Pt(111), Pd/Au(111) and Ru(0001). For Ru, also the work function change induced by the half-dissociated water layer is included.

Yet it is known that the work function of many metal surfaces is significantly reduced upon the adsorption of water bilayers [1, 41]. In figure 2, we have plotted the calculated work function changes for H-down and H-up water bilayers on Au(111), Ag(111), Pt(111), one Pd monolayer on Au(111) and Ru(0001). For Ru, we also determined the work function change induced by the half-dissociated water layer.

First of all it is obvious that the water-induced work function change sensitively depends on the orientation of the water bilayer. The difference in the induced work function change between the H-up and the H-down configuration is about 2 eV for all considered metal substrates. A similar result has recently been obtained in periodic DFT calculations for water bilayers on Pd(111) [31]. These findings are not surprising considering the fact that the two types of water bilayers should have opposite dipole moments normal to the surface.

What is indeed surprising is the fact that there is a strong asymmetry in the induced work function change for both orientations of the water bilayers. For Pt(111), Pd/Au(111) and Ru(0001), the work function is even lowered due to the presence of the water bilayers irrespective of their orientation. Naively one would expect that the H-down bilayer increases and the H-up bilayer lowers the work function by the same amount because of their opposite dipole moments. Instead, there is an overall tendency to lower the work function that rises with increasing interaction strength between water and the metal (note that the overlayer system Pd/Au(111) binds water as strongly as Pt(111) [22] due to a combination of strain and electronic interaction effects [42]–[44]).

In order to understand the electronic origin for these findings, we have analyzed the water-induced electron density difference on Pt(111)

$$\Delta\rho = \rho(\mathrm{H_2O/Pt(111)}) - (\rho(\mathrm{H_2O}) + \rho(\mathrm{Pt(111)})), \tag{1}$$

which corresponds to the interaction-induced rearrangement of the electron density. In figure 3, we have plotted the laterally averaged $\Delta\rho$ for the H-down and the H-up bilayer as a function

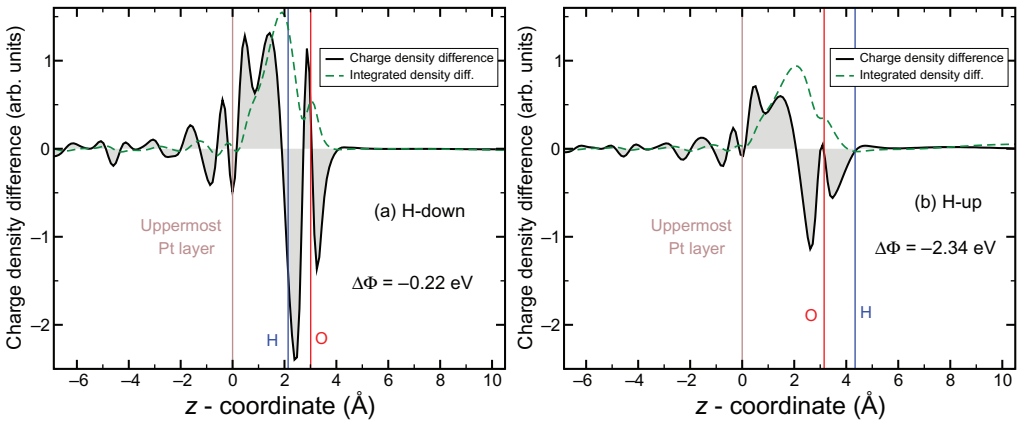

Figure 3. Laterally averaged electron density difference upon the adsorption of an H-down (a) and an H-up (b) water bilayer on Pt(111) as a function of the vertical height. The heights of the uppermost Pt layer and the hydrogen and oxygen atom of the oppositely oriented water molecules are indicated by vertical lines. In addition, the integrated charge density difference is plotted. Note the same scale for the charge density difference in both figures.

of the vertical height. Note that for both orientations of the water bilayer there is a significant electronic charge transfer from the region of the water bilayer toward the space between the uppermost metal layer and the water molecules, as has in fact also been found before for water layers on Ru(0001) [39]. In the case of the H-down water bilayer, this charge transfer is more pronounced than for the H-up bilayer. Note that this transfer leads to the creation of an additional dipole layer with a dipole moment that reduces the work function. For the H-down bilayer, this overcompensates the effect of the intrinsic dipole moment of the water bilayer leading to a net work function reduction on Pt(111), whereas for the H-up bilayer, these two dipole moments add up.

This strong charge rearrangement is a consequence of the high polarizability of water which is reflected by the large dielectric constant of water. We also analyzed the local charge rearrangement. Figure 4 shows charge density difference isosurfaces around the water molecules of the H-down bilayer on Pt(111). Interestingly enough, the H-down molecules are much more polarized toward the surface than the water molecules oriented parallel to the surface, in agreement with previous results [7], although an isolated water monomer binds through its oxygen atom. The same is in fact true for the H-up water molecule of the H-up layer which also shows a larger polarization than the flat-lying water molecules. Actually, the charge rearrangement is similar on all investigated metals, but on Au(111) and Ag(111) it is smaller than on Pt(111), Ru(0001) and Pd/Au(111).

Previous first-principles studies of the water adsorption on metal substrates have focused on charge density difference profiles [6, 7, 9, 39] and the partial density of states projected onto the water molecules [9, 39] in order to analyze the bonding of water to metal surfaces, but they have not paid special attention to the change of the local density of states (LDOS) of the uppermost metal atoms of the surface. Figures 3 and 4 indicate that there is charge rearrangement inside the metal substrate which is, however, rather moderate compared with the change at the water molecules. We note that similar effects have also been found in the surprisingly large reduction of the work function induced by ultrathin oxide layers on metal surfaces [45].

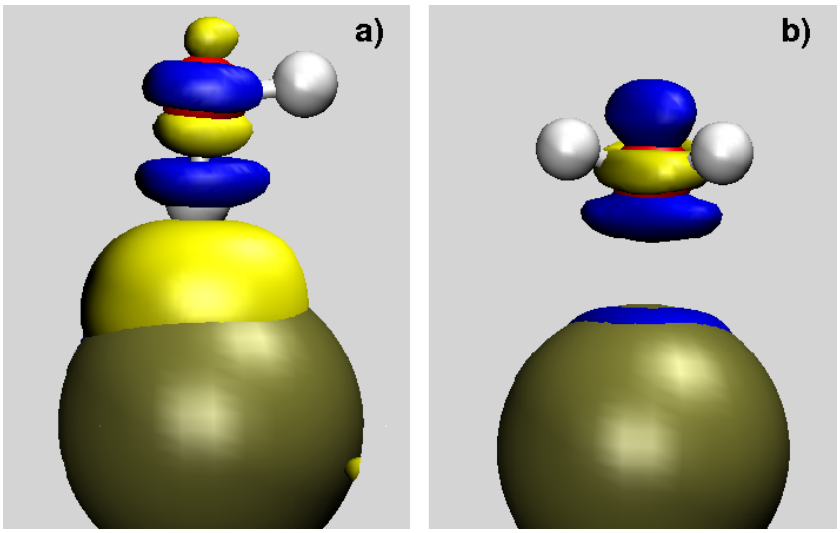

Figure 4. Isosurface plot of the charge density difference for a H-down bilayer on Pt(111) around the water molecule with the hydrogen atom down (a) and in the parallel configuration (b). Yellow colors denote charge accumulation, blue colors charge depletion.

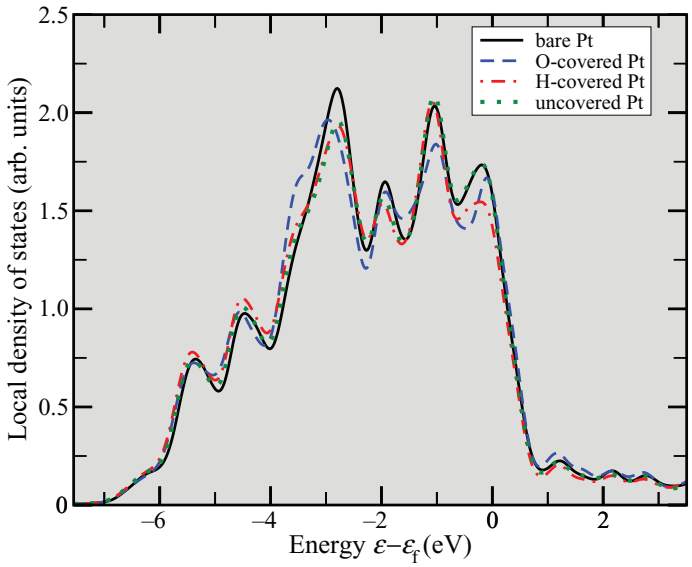

Figure 5. LDOS of the Pt(111) surface atoms without and in the presence of water. For the H-down water bilayer, the LDOS of the three inequivalent Pt atoms within the surface unit cell is shown (after [30]).

Furthermore, as figure 5 demonstrates, the water-induced change of the LDOS in the uppermost layer of Pt(111) is also rather small. In figure 5, the LDOS of the three inequivalent Pt surface atoms per $\sqrt{3} \times \sqrt{3}R30^\circ$ surface unit cell of the water-bilayer-covered surface are compared with that of the bare Pt(111). There are only slight changes in the peak heights. For example, there is an additional shoulder in the LDOS at about -3.5 eV for the Pt atom

located below an O-bonded water molecules reflecting some Pt–O interaction. Still, the peaks are practically not shifted upon the adsorption of the water layer indicating a rather weak interaction.

With respect to the small change of the LDOS of the uppermost Pt atoms upon the adsorption of a water layer [30] we therefore stress that the charge rearrangement shown in figure 3 should not be regarded as a charge transfer to the surface, but rather as a charge transfer to the region between metal substrate and water layer. As a consequence, the presence of water leads only to small changes in chemisorption energies of additional adsorbates [22, 46]. This analysis also shows that there is no need to invoke water molecules bonded with the oxygen end down in order to explain the substantial water-induced work function change of metal surfaces, as was done previously [1].

Experimentally, water-induced work function changes of −0.6 eV on polycrystalline Au films [41], of about −1.0 eV on Pt(111) [47, 48] and about −1.3 to −1.4 eV on Ru(0001) at temperatures below 140 K [49, 50] were found. Interestingly enough, all these numbers lie in between our calculated values for the H-down and the H-up water bilayers. This indicates that in the experiments there were no pure water bilayers present because properties of adsorption systems such as work function changes are usually reliably reproduced in DFT calculations [51]. Since the work function measurements are usually carried out at cryogenic temperatures [1], the thermal motion of the water molecules should be limited. Hence either some other water structure is formed upon the sequential water exposure, or mixtures of H-down and H-up phases are present which seems to be reasonable considering the similar adsorption energies of both configurations. We will show below that the thermal motion of the water bilayers indeed leads to a work function with intermediate values between those of the H-up and the H-down water bilayer.

4. Water–metal interface at room temperature

Many of the surface science studies addressing the structure of water at metal surfaces have been performed at temperatures far below the freezing point of water [1, 2] in order to get a better structural information that is not influenced by thermal fluctuations. However, from a practical point of view the structure of water–metal interfaces at room temperature is much more relevant because this corresponds to the conditions under which typically processes in corrosion, biology or electrochemistry occur.

There have been plenty of molecular dynamics studies using classical interaction potentials of the force-field type. Although these potentials can describe the water–water interaction quite well [17, 19], the metal–water interaction might be less reliably reproduced due to the fact that force fields do usually not describe the many-body nature of metal bonding correctly. Here embedded atom methods [52] are better suited, but they cannot be easily coupled to the force-field description of the water–water interaction. Hence AIMD simulations based on DFT calculations addressing the structure of the metal–water interface at room temperature should be the appropriate method because they combine an accurate representation of the electronic and structural properties of metal surfaces [51] with a satisfactory description of the bonding of water molecules [20, 34, 35].

There have been already AIMD simulations addressing the structure of water at Cu(110) [4] and Ag(111) [5], the vibrational properties of water in the bilayer structure at Ru(0001), Rh(111), Pd(111) and Au(111) [6, 7], the coadsorption of water and hydroxyl on Rh(111) [53],

or oxidation reactions in the presence of water [54]. However, these studies were hampered by the high computational costs of AIMD simulations resulting in relatively short simulation times and/or small simulation cells.

In detail, the Cu(110)–water interface [4] and the Ag(111)–water interface [5] were addressed by Car–Parrinello molecular dynamics simulations with the metal atoms being fixed at their unrelaxed surface geometries. More than one layer of water atoms was used in the simulations, and the starting geometry of the Car–Parrinello simulations was determined using a classical water–metal model potential [17]. After a thermalization period of about 1 ps, the *ab initio* production runs were carried out for about 2 ps at a temperature of 300 K. No hexagonal ice-like water layer was observed. However, for the Ag(111)-water simulations, a rectangular $c(8 \times 4)$ surface unit cell was chosen, which does not allow the formation of a hexagonal water layer.

Further AIMD studies focusing on the structure and vibrational spectra of water at Ru(0001), Rh(111), Pd(111) and Au(111) were performed within a $\sqrt{3} \times \sqrt{3}R30^\circ$ geometry at temperatures of 90–140 K for a run time of 2 ps after an equilibration time of about 1 ps [6, 7]. These simulations allowed an assignment of vibrational modes in agreement with experimental observations at low temperatures [55]. However, the small unit cell and the low temperatures did not allow any significant restructuring of the water layer.

Yet, due to the improvement in computer power and the development of more efficient electronic structure algorithms AIMD simulations can nowadays yield statistically significant results [56]. We have therefore performed AIMD simulations of water bilayers at close-packed metal surfaces within a larger $2\sqrt{3} \times 2\sqrt{3}R30^\circ$ surface unit cell and longer simulation times of at least 8 ps at room temperature. The simulations were started with the energy minimum structure and random initial velocities. A second water layer was placed on top of the first one in order to model a surrounding water environment. To prevent desorption of this second, weakly bound water layer, two oxygen atoms of the eight water molecules of the second layer in the unit cell were fixed vertically. In the results discussed below, however, we will solely focus on properties of the first water layer.

Figure 6 shows snapshots of the first water layer on the considered metal substrates. On Ag(111) and Au(111), where the water bilayer is most weakly bound among the considered substrates, the ice-like hexagonal structure is basically broken up after 8 ps. Instead, an open structure has evolved with stripes of water molecules forming and a larger region uncovered by water molecules.

On Pt(111) and Ru(0001), the configuration of the single water molecules is also no longer well ordered, the structure does neither correspond to a H-up nor to a H-down configuration. Still the hexagonal ice-like structure is intact, as can be seen if one focuses on the uncovered substrate atoms. The half-dissociated water layer on Ru(0001) stays almost perfectly intact, which can be understood considering the strong OH–Ru interaction so that the immobile hydroxyl groups act as an anchor for the water structure. On Pd/Au(111), the structure looks also somewhat disordered. Note that the selection of these images might be misleading since snapshots could depict singular events. However, we have made sure that the snapshots shown in figure 6 really correspond to typical configurations that are characteristic for the emerging structures.

To obtain some insights into the movement of the single water molecules, we have plotted in figure 7 the trajectories of the corresponding oxygen atoms. The single oxygen atoms were color-coded to allow the identification of their traces. On Ag(111) and Au(111), the water molecules possess a considerable mobility on the surface. The breaking up of the ice-like

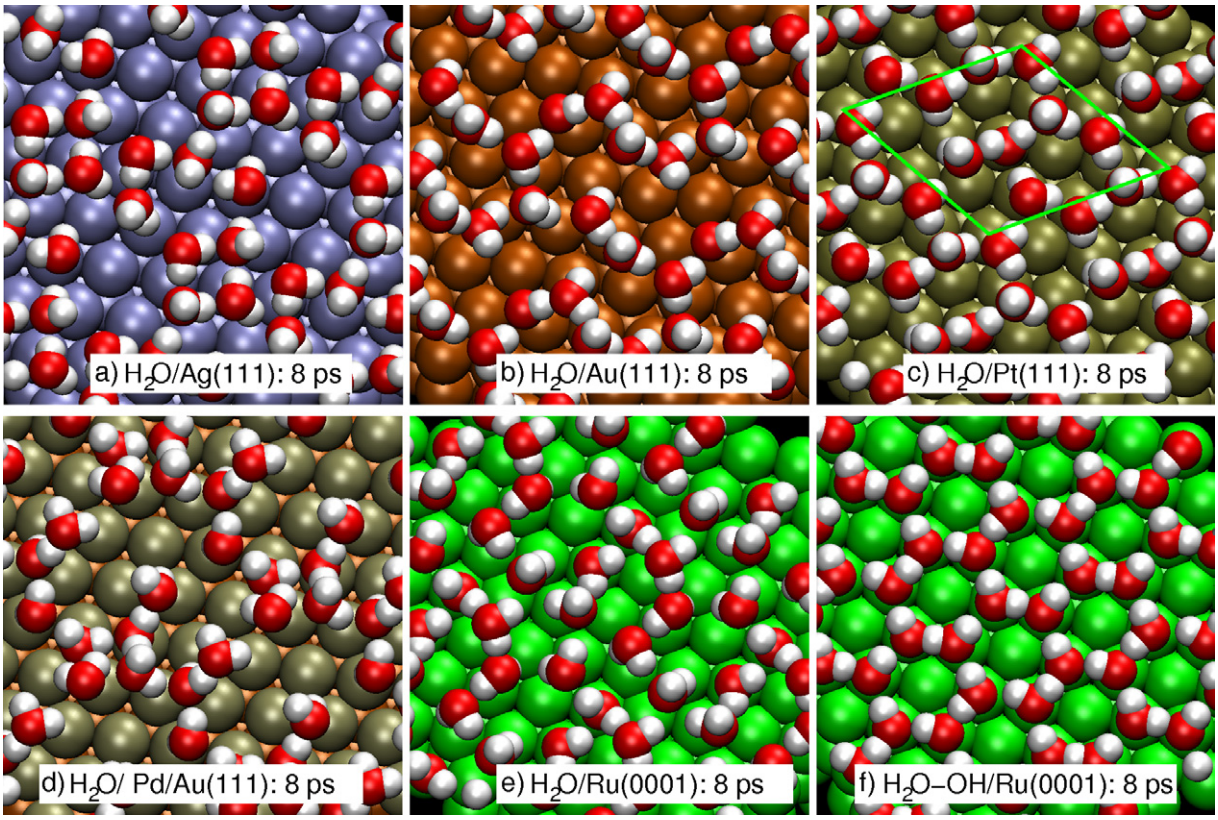

Figure 6. Snapshots of the structure of the water bilayer taken from the AIMD simulations of water at 300 K on (a) Ag(111), (b) Au(111), (c) Pt(111), (d) Pd/Au(111) and (e) Ru(0001). Panel (f) shows the structure of the half-dissociated water layer on Ru(0001) with the additional hydrogen atoms being removed. The snapshots were taken after 8 ps. In panel (c), the surface unit cell is indicated.

structure is reflected by the fact that some of the water molecules leave their original adsorption sites. On the three other surfaces where the water layer is more strongly bound, the water molecules stay relatively localized and remain close to their initial positions, although they exhibit some quite strong fluctuations. Now it also becomes obvious that on Pd/Au(111) the hexagonal water structure is more or less preserved in spite of the disordered impression of the AIMD snapshot after 8 ps.

Note that the chosen unit cell imposes constraints on the possible structures that can evolve. A surface unit cell compatible with the hexagonal ice-like structure might always artificially favor the bilayer structure. Hence, the result that the hexagonal water structure stays intact on Pt(111), Pd/Au(111) and Ru(0001) in the simulations might still be an artefact of the chosen periodicity. However, the fact that on Ag(111) and Au(111) this structure does not stay intact is a strong indication that the ice-like bilayer structure is indeed thermodynamically not stable at room temperature.

The difference between the water structures on the inert surfaces and the more reactive surfaces is also reflected in the wall–oxygen distribution functions $g_\gamma(z)$ plotted in figure 8. For the more strongly interaction substrates Pt(111), Pd/Au(111) and Ru(0001) two distinct

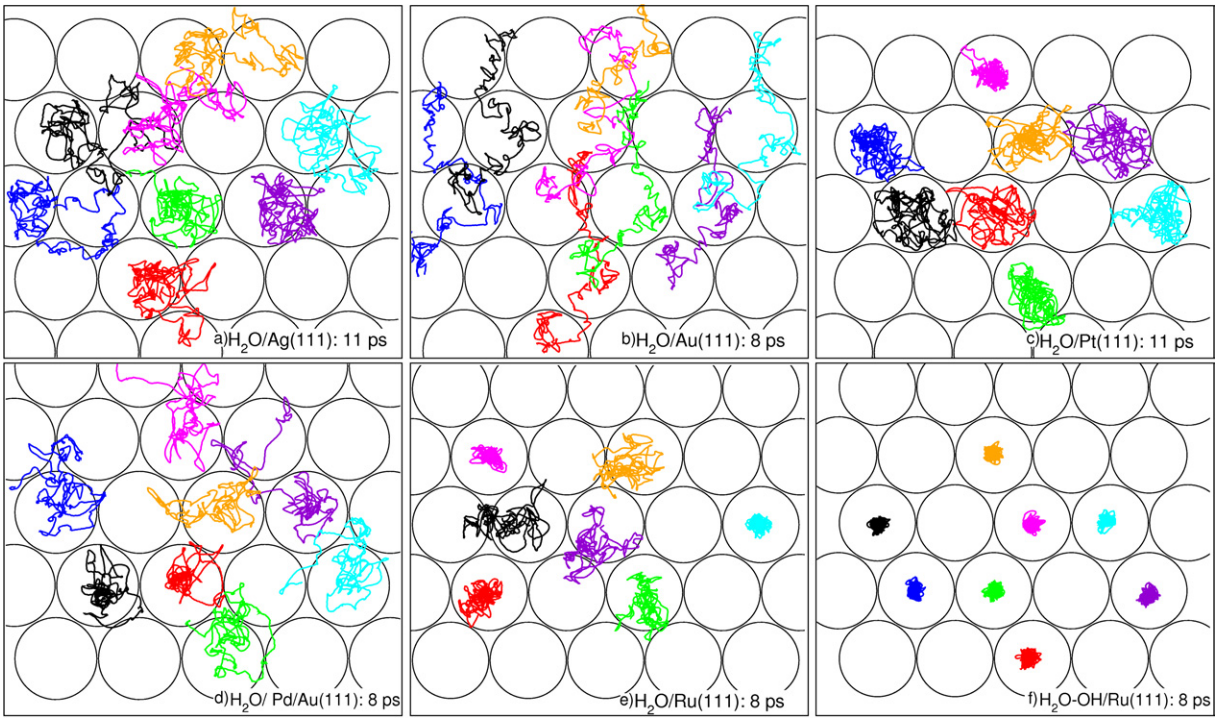

Figure 7. Trajectories of the oxygen atoms of the water molecules taken from the AIMD simulations of water at 300 K on (a) Ag(111), (b) Au(111), (c) Pt(111), (d) Pd/Au(111) and (e) Ru(0001). Panel (f) corresponds to the structure of the half-dissociated water layer on Ru(0001) with the additional hydrogen atoms being removed. The trajectories of the different oxygen atoms have been color-coded so that the movement of single water molecules can be followed.

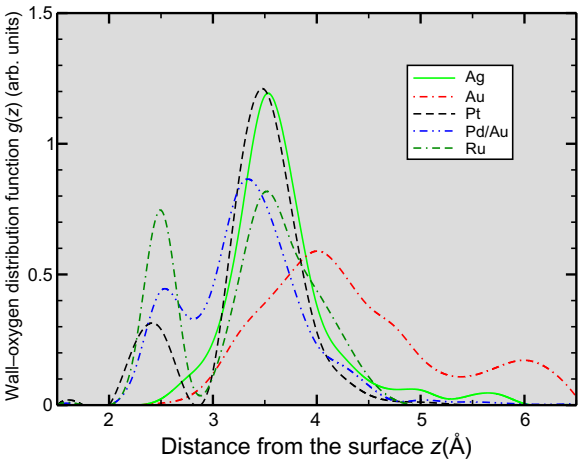

Figure 8. Wall–oxygen distribution function obtained from the AIMD simulations of water on Ag(111), Au(111), Pt(111), Pd/Au(111) and Ru(0001).

peaks are found at distances of 2.5 and 3.5 Å from the surface whereas for the noble metal substrates only one peak is found. The small peaks closer to the surface correspond to water molecules oriented parallel to the surface and bound via their oxygen atom which in fact is the most favorable configuration of the water monomer on metal surfaces [9]. So interestingly, at the metal–water interface with Ag or Au as the substrate the water molecules are hardly found in the configuration that corresponds to the energy minimum configuration for isolated adsorbed water molecules.

Thus, the existence of the peak closer to the surface at 2.5 Å is clearly correlated with the interaction strength between water and the metal substrate. In addition to the strength of this interaction, however, also the lattice constant of the underlying substrate has to be considered for a full understanding of the resulting structures. Note that the trajectories of the water molecules (figure 7) and the wall–oxygen distribution (figure 8) look similar for Pt(111), Pd/Au(111) and Ru(0001), however, according to the snapshots the water configurations seem to be much more ordered on Pt(111) than on the other strongly interacting substrates. Among these three substrates, the lattice spacing of Ru fits best to the equilibrium value for the lattice constant of ice I_h [9]. However, it is quite probable and supported by our analysis of the charge density differences that the relatively strong interaction between water and Ru weakens the water–water bonds leading to effectively compressed water rings. On Pd/Au(111), on the other hand, the hexagonal water structure is under tensile strain because of the large Au lattice constant. The Pt surface might have in fact a more appropriate spacing for the hexagonal water structures. Therefore the water bilayer on Pt(111) retains its bilayer-like structure most closely under thermal conditions while both the compression as well as the expansion cause a stronger variation in the orientation of the water molecules at room temperature. Still the water molecules stay close to their on-top adsorption sites.

Experimentally, the direct determination of the exact structure of water at the solid–liquid interface is hard to achieve. One indirect way to derive the water structure is to measure vibrational spectra. In particular, sum-frequency generation (SFG) is well suited for this purpose since it is sensitive to the interface. In a recent SFG study, the vibrational spectra of water on Pt(111) and Au(111) were analyzed at room temperature in an electrochemical setup as a function of the electrode potential [57], in particular focusing on the O–H stretch vibration in the range between 2800 and 3800 cm^{-1}.

To analyze the spectra one has to consider the following fundamental aspects of water vibrations [58]: a water monomer has symmetric and antisymmetric OH stretching modes ν(OH) at 3720 and 3660 cm^{-1} and a HOH bending mode δ(HOH) at 1595 cm^{-1}. Upon hydrogen-bonding to other molecules or the substrate, the ν(OH) modes are red-shifted and become broader, while δ(HOH) modes are blue shifted. It is furthermore known that the ν(OH) modes are remarkably red shifted for water molecules that are hydrogen bonded to other water molecules by donating hydrogen atoms, while the shift is weaker for hydrogen acceptors.

O–H stretch vibrations at about 3400 cm^{-1} have typically been assigned to three-fold coordinated water, i.e. water in a disordered liquid-like structure, whereas OH stretch vibrations at about 3200 cm^{-1} have been taken as a signature of four-fold coordinated water, i.e. highly ordered ice-like water molecules [59].

In the SFG experiments, for Pt(111) two broad peaks at 3200 and 3400 cm^{-1} were obtained [57], while on Au(111) the observed vibrational spectra were dominated by a broad peak around 3500 cm^{-1}. This peak, however, was attributed to oxide formation. The results

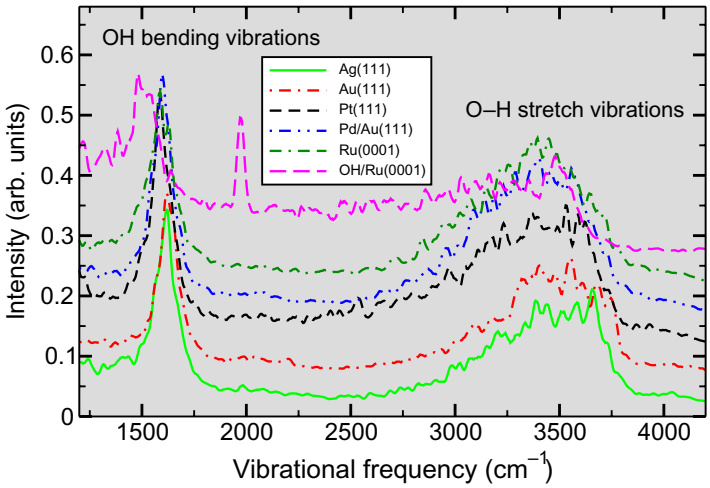

Figure 9. Vibrational spectra of water bilayers on Ag(111), Au(111), Pt(111), Pd/Au(111) and Ru(0001) and of the half-dissociated water layer on Ru(0001) obtained from the AIMD runs using the Fourier transform of the velocity–velocity autocorrelation function. The spectra have been averaged over ten different starting points.

were interpreted as being an indication that on Pt(111) ordered and disordered water structures coexist whereas on Au(111) the water is less well ordered.

The snapshots shown in figure 6 indicate that this interpretation is consistent with the qualitative analysis of the resulting structure of the AIMD runs. For a more quantitative comparison with the experiment, we have derived the vibrational spectra of the water bilayers from the Fourier transformation of the velocity auto-correlation function [60] which are plotted in figure 9. The run time of the simulations corresponds to a spectral resolution of less than $\delta\omega \sim 5\,\mathrm{cm}^{-1}$ [60].

Two main peaks are visible in the calculated spectra, around $3500\,\mathrm{cm}^{-1}$ and around $1600\,\mathrm{cm}^{-1}$. These are related to the OH stretch and bending vibrations, respectively. First of all it is obvious that the water vibrations on Pt(111), Pd/Au(111) and Ru(0001) are shifted to lower frequencies compared with those on Au(111) and Ag(111).

These findings can be explained by the stronger interaction between water and the more reactive substrates Pt, Pd/Au and Ru than between water and the noble metals Ag and Au. The spectra are similar to the corresponding experimentally measured spectra on Pt(111) and Au(111) [57], in particular as far as the existence of a broad peak structure in the O–H stretch region on Pt(111) is concerned. Note that the upper part of the O–H stretch peak at about $3400\,\mathrm{cm}^{-1}$ had been assigned to the presence of a disordered water structure on the surface. In our simulations, the hexagonal ring-like structure of the water molecules is still preserved at room temperature, but still we find a significant intensity around $3500\,\mathrm{cm}^{-1}$. A closer inspection of figures 6 and 7 reveals that the water molecules, although they stay close to their initial on-top sites, strongly vibrate and rotate around their equilibrium configurations leading to a significant fraction of temporarily low-coordinated water molecules which explains the high O–H stretch frequencies found in our simulations.

On Au(111), where a disordered water structure evolves at room temperature, higher O–H stretch frequencies are found which can be rationalized by the fact that in the open structure

many water molecules tend to be low coordinated with hydrogen atoms pointing into empty space as seen in figure 6.

The vibrational spectrum of water on Pd/Au(111) is similar to the spectra on Pt(111) and Ru(0001). This seems to be surprising since in the analysis of the trajectories clearly a disordered open character of the water layer like on Ag(111) and Au(111) is found. However, as already discussed above and shown in figure 7, the water molecules stay close to their equilibrium on-top sites on Pd/Au(111), and the disordered look is due to significant fluctuations in the molecular orientation because of the large lattice constant of the underlying Au substrate. Hence, it is not necessarily right to conclude a strictly ordered water arrangement from a broad peak in the vibrational spectrum around 3200 cm^{-1}. It is still debated whether the OH vibration modes at 2700–3000 cm^{-1} can be assigned to the vibration of a water molecule hydrogen bonded to the metal surface or to a distorted OH $\cdots$ O bond [61]–[63]. We are not able to definitely clarify this question from our calculations but from analyzing explicit OH vibrational amplitudes we suppose that both effects are present.

As far as the vibrational spectrum of the half-dissociated water bilayer is concerned, it is obvious that it is distinctly different from the spectra of the intact bilayers: both the OH bending and the O–H stretch vibrations are significantly red shifted, there is a broad featureless background between the peaks for the bending and the stretch vibrations, and there is an additional sharp peak at 2000 cm^{-1}. Such an additional mode has already been predicted in a DFT study in which the vibrational modes were derived from the dynamical matrix [64]. Based on a Fourier analysis of the H–Ru distances, we assign this mode to the H–Ru vibrations of the isolated hydrogen atoms at the top site. This assignment is also consistent with the results of a recent DFT study on hydrogen adsorption on Ru(0001) [65]. In the experiment, however, the hydrogen atoms might not stay at the top sites since this mode has not been observed at conditions at which the half-dissociated water layer should be formed. In fact, under these conditions only a single OH bending mode has been measured [66]. The absence of the OH stretch and bending modes in the experiment, however, is not surprising considering the fact that the molecules in the half-dissociated bilayer are no longer adsorbed in an upright, dipole active geometry on the surface [66] but oriented parallel to the surface, as figure 1(c) demonstrates.

Finally, we like to address the work function of the thermalized water layers. In figure 10, we have plotted the time evolution of the calculated work function change for water-covered Ru(0001) derived from the AIMD runs starting initially with the H-up and H-down water bilayer configurations on Ru(0001). Due to the thermal reorientation of the water molecules, the work functions become very similar in both AIMD runs. This shows that at thermal conditions the distinction between H-up and H-down bilayers is hardly possible. Recent experiments demonstrated that water on Ru(0001) becomes partially dissociated only at temperatures above 140 K [67]. The measured work function changes at temperatures below 140 K [49, 50] are reasonably close to our calculated mean value of the work function change in figure 10 of about -1.5 eV whereas the half-dissociated layer on Ru(0001) leads to a much smaller work function change (see figure 2). This indicates that the work function changes measured below 140 K were obtained from intact water bilayers on Ru(0001) which do neither correspond to an H-up nor to an H-down structure but to a orientationally disordered hexagonal structure. Our calculated vibrational spectrum for the intact water bilayers on Ru(0001) also agrees nicely with the measured one for a water bilayer deposited at 145 K [66]. Furthermore, the observed increase in the work function upon heating the system [49] is consistent with the formation

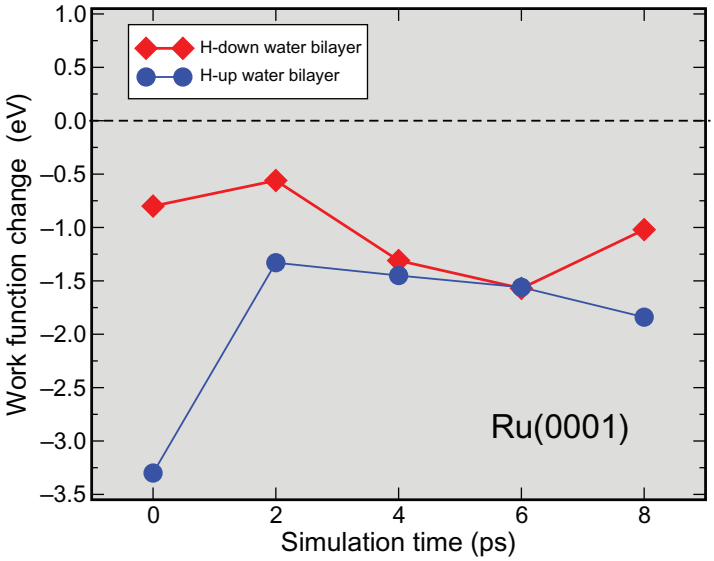

Figure 10. Time evolution of the work function in the AIMD runs of H-up and H-down water bilayers on Ru(0001).

of the half-dissociated water layer on Ru(0001) whose work function is significantly higher compared with the intact bilayer systems (see figure 2).

In addition, thermal fluctuations then also explain the fact that for water on Pt(111) and Au(111) work functions changes were measured [41, 47, 48] that are intermediate between the calculated values for H-up and H-down water bilayers.

5. Water–metal interface in the presence of electric fields

The water–metal interface is of special interest in electrochemistry because in electrochemical systems the electrolyte in contact with the electrodes often corresponds to an aqueous system. However, the presence of external electric fields or varying electrode potentials adds considerable complexity to the theoretical treatment of the electrochemical water–metal interface, in particular in periodic DFT codes.

In an electrochemical cell, the electrostatic potential falls off at the solid/liquid interface within the so-called double layer to a constant value in the electrolyte [68]. In electrochemical experiments, typically the electrode potential is specified which results in the creation of a non-vanishing surface charge density at the metal electrode. The amount of the surface charge is controlled by the capacity of the double layer, which depends on its structure. Thus it is the potential that is the crucial variable in the simulations of electrochemical systems so that the calculations should be performed at constant chemical potential of the electrode rather than at constant charge. Yet, calculations addressing the electrochemical metal–water interface are typically performed at constant charge because this is usually computationally less demanding. Still, in periodic calculations the unit cell has to be neutral, i.e. there must not be a net charge per unit cell because otherwise the electrostatic energy diverges. Hence the excess charge has to be balanced by counter charges.

Electric fields in periodic DFT calculations can easily be introduced by including a dipole layer in the vacuum region between two slabs [69]. This approach has for example been used

to study the electric field induced flip of water molecules from the H-down configuration to the H-up geometry [22] which has been observed experimentally [70, 71]. This approach does not introduce any excess charges so that charge neutrality is maintained, but it is not straightforward to relate the applied dipole field to the corresponding electrode potential.

Instead of including a dipole layer, a counter electrode may be explicitly considered, for example as a localized planar charge distribution with a Gaussian profile perpendicular to the surface [25], [72]–[75] or by putting a perfect conducting continuum with a non-vanishing surface charge above the slab in a two-dimensional periodic approach [25, 28, 29]. Thus the reconstruction of charged surfaces [72, 73, 75] or the structure of water under acidic conditions [28, 29] was addressed. In order to determine the electrode potential in this approach, the charge can be related to the potential via experimentally derived capacities [73] or in the presence of several water layers from the potential profile inside of the water bulk region [29].

In periodic DFT codes, it is typically a default procedure to introduce a homogeneous charge background when charged systems are considered in order to avoid the divergence of the electrostatic energy. This approach does usually not require any substantial programming efforts. However, there are certain issues to be considered when a homogeneous background is added to a system. First of all, a homogeneous charge background might introduce artefacts to the one-electron potential. Naively one could think that a uniform charge background cannot lead to additional variations in the potential equivalent to introducing an additional electric field because it is translationally invariant. However, one has to take into account that the constant charge background is superimposed on the varying charge density of the water–metal system, and the resulting electrostatic potential as a solution of the Poisson equation is a consequence of the whole charge distribution subject to the appropriate boundary conditions. In particular, in vacuum regions where the charge distribution is entirely given by the uniform background charge, this can lead to a quadratically varying potential [24] since the solution of the Poisson equation for a region with a constant charge background

$$\nabla^2\phi(\mathbf{x}) = 4\pi\rho_{\mathrm{o}} \tag{2}$$

has the general solution in Cartesian coordinates

$$\phi(\mathbf{x}) = 2\pi\rho_{\mathrm{o}}\left(\sum_{i,j=1}^{3} C_{ij}x_i x_j + \sum_i C_i x_i + C_0\right) \tag{3}$$

with $\sum C_{ii} = 1$. The influence of this artefact is strongly reduced in regions where polarizable atoms and molecules are present due to screening effects. This can indeed be the case at the metal–water interface [24], which makes this approach applicable for the description of electrochemical interfaces.

Secondly, the uniform charge background interacts with the system under consideration. Therefore the total energy E_{DFT} resulting from the periodic DFT calculations has to be corrected. It can be shown [23, 24] that this correction involves an integration over the charge according to

$$E = E_{\mathrm{DFT}} + \int_0^q \left[\int \frac{V_{\mathrm{tot}}}{\Omega}\,\mathrm{d}^3x\right]\mathrm{d}Q, \tag{4}$$

where V_{tot} is the total electrostatic potential of the charged water/electrode system including the uniform charge background, and Ω is the size of the unit cell.

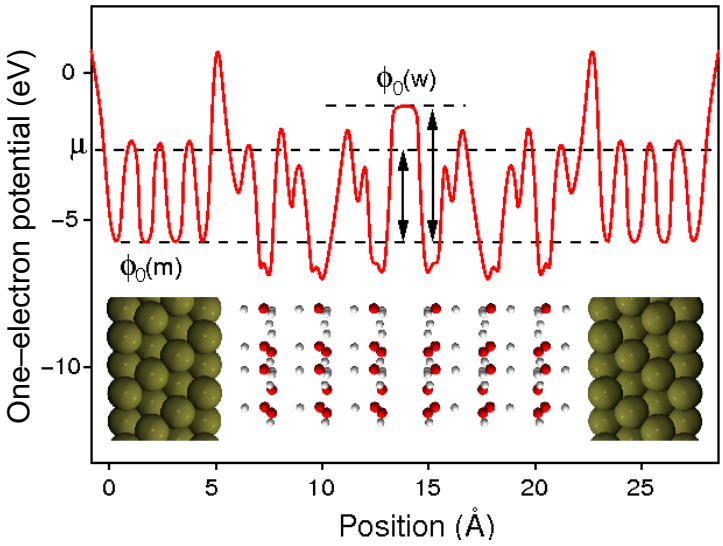

Figure 11. Schematic illustration of the electrostatic energy profile across the unit cell in a periodic slab calculation for solvated metal slabs. μ_e is the chemical potential of the electrons which corresponds to the Fermi energy at $T = 0\,\mathrm{K}$. $\phi_0(\mathrm{m})$ is a bulk metal potential that can be used as a reference for the other potentials (after [24]).

As already mentioned, in electrochemical experiments typically the electrode potential is controlled and not the charge. As far as the calculations for a given charge are concerned, it is therefore crucial to specify a well-defined reference potential that allows a meaningful comparison with electrochemical experiments performed under potential control.

If the whole supercell is filled with the metal slabs and the water molecules, then it is hard to define an absolute value for the one-electron potential, for example with respect to the vacuum level. Taylor *et al* have suggested a so-called 'double-reference method' [24] for the situation in which the charge of the slab is compensated by a uniform background. In a first step, a DFT calculation is performed for a solvated slab with a vacuum region introduced in the middle of the unit cell between the slabs. The water layer should be thick enough that the vacuum level is converged with respect to the number of included water layers. For such a setup, the vacuum level ϕ_∞ and the work function of the metal–water interface are computationally well defined, as in periodic calculations for the metal–gas interface.

Then a point in the interior of the metal slab is selected where the potential variation does not depend on the presence of the vacuum region and its potential and its value $\phi_0(m)$ is specified with respect to the vacuum level. Further calculations are performed with the region between the metal slabs filled with water, as illustrated in figure 11, and all other potentials are taken with respect to $\phi_0(m)$.

For a charged slab, however, the variation in the electronic charge q leads to the existence of electric fields throughout the whole supercell. Consequently, a vacuum reference point cannot be established because there is no region where the potential is flat. The following procedure was suggested to handle this problem [24]: a region far from the electrode is fixed at its position in the $q = 0$ calculation and its potential $\phi_0(w)$ (see figure 11) is used as the second

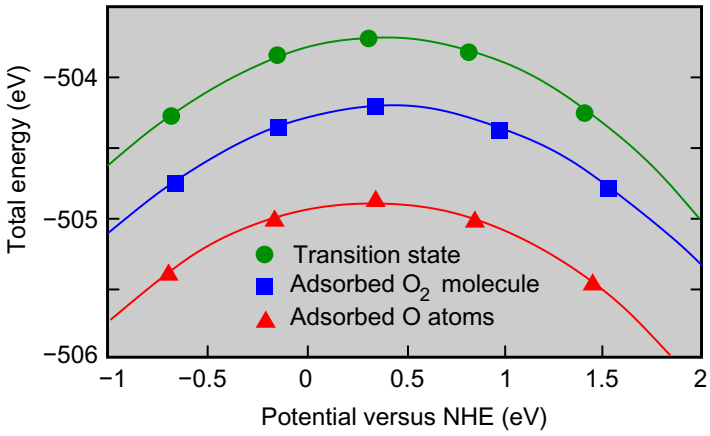

Figure 12. Total energies versus potential for the initial, transition and final state of O_2 dissociation on solvated Pt(111). The symbols correspond to the results obtained for different charge states of the Pt electrode with a charge of -1, -0.5, 0, 0.5 and $1e^-$, respectively, added to the supercell and compensated by a uniform charge background. The solids curves are quadratic fits to the results (after [76]).

reference point. The rest of the system is then relaxed under the influence of the applied charge, and the potential at all other positions is shifted with respect to the second reference point.

It is important to realize that there is a difference between calculations at constant charge and at constant potential. Along a certain reaction path the geometry of the reactants changes. This modifies the electron distribution and the corresponding dipole moments and thus in general also alters the work function of the electrode that is directly related to the electrode potential. Thus the different configurations along a reaction path calculated for a constant value of the charge do not necessarily correspond to the same electrode potential.

This is illustrated in figure 12 using the dissociation of O_2 on a solvated Pt(111) slab as an example [76]. As already mentioned, it is more convenient to perform periodic electronic structure calculations for a specified charge of the system. The symbols in figure 12 correspond to the energies of the initial, transition and final state of the O_2 dissociation obtained with a charge of -1, -0.5, 0, 0.5 and $1e$, respectively, added to the supercell and compensated by a uniform charge background. The respective potentials were obtained using the double-reference method, and the solid lines are quadratic fits to the results. For symbols aligned vertically above each other, the dissociation barrier would be the same in the constant charge and in the constant potential mode. However, as figure 12 reveals, this is in general not the case, in particular at positive potentials, due to the rearrangement of the atoms along the reaction path.

Instead of charging the system, neutral atoms or molecules that act as electron donors or acceptors might be explicitly added to the water layer. This can for example been achieved by introducing additional hydrogen atoms to the water–metal interface [26, 77]. The added hydrogen atoms become solvated as protons whereas the electrons move to the metal electrode. By changing the hydrogen concentration, the surface charge and hence the electrode potential can be varied. In this approach, the whole supercell remains neutral so that no countercharges are needed.

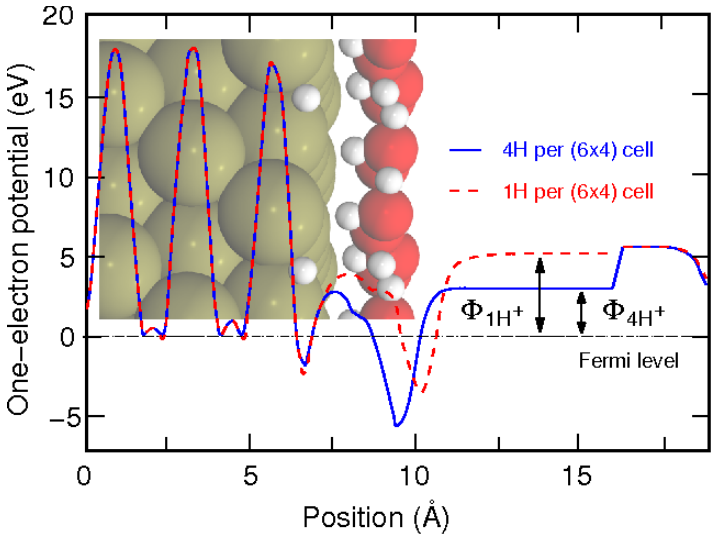

Figure 13. One-electron potential averaged in lateral direction as a function of the position along the surface normal for two different hydrogen coverages resulting in two different electrode potentials. In the vacuum layer, there is a potential drop due to the presence of a dipole layer (after [26]). The structure of the interface with additional protons is illustrated in the inset.

This method is illustrated in figure 13. The hydrogen coverage influences the work function and thus also the corresponding electrode potential. This method has been applied to identify the mechanism of the hydrogen evolution reaction on Pt(111) [26, 77]. The fine-tuning of the electrode potential, however, demands relative large surface unit cells in order to adjust the required hydrogen coverage. Furthermore, there is a rather large gap in the possible electrode potentials once the coverage becomes larger than unity [26].

In order to estimate the influence of a variation of the electrode potential on the structure of the water layer on metal electrodes, we have performed AIMD simulations in the constant charge mode for a charged slab with the excess charge being compensated by an uniform charge background. In detail, for Ag(111) and Pt(111) as a substrate we have performed AIMD simulations in which a charge of 0.4 electrons was added (denoted by $+0.4e^-$) or subtracted (denoted by $-0.4e^-$), leading to a negatively or positively charged electrode, respectively. Such a charge leads to changes in the electrode potential within the chosen surface unit cell of up to 0.5 eV, as can for example been seen in figure 12. This is large enough to make characteristic structural modifications as a consequence of the variation in the electrode potential detectable. In analogy to the situation depicted in figure 12, the thermal motion of the water molecules leads to a varying dipole moment and thus to a varying electrode potential. Hence we have made no attempt to determine the corresponding electrode potential; instead, we will focus on qualitative trends induced by the charging of the electrodes.

In figure 14, we plotted the oxygen–wall distribution function for water above the negatively and positively charged Ag(111) and Pt(111) substrates. We first concentrate on the results for the charged Pt substrates. For the positively charged surface, the peak closer to the substrate corresponding to the oxygen atom of the flat lying water molecule increases. This can

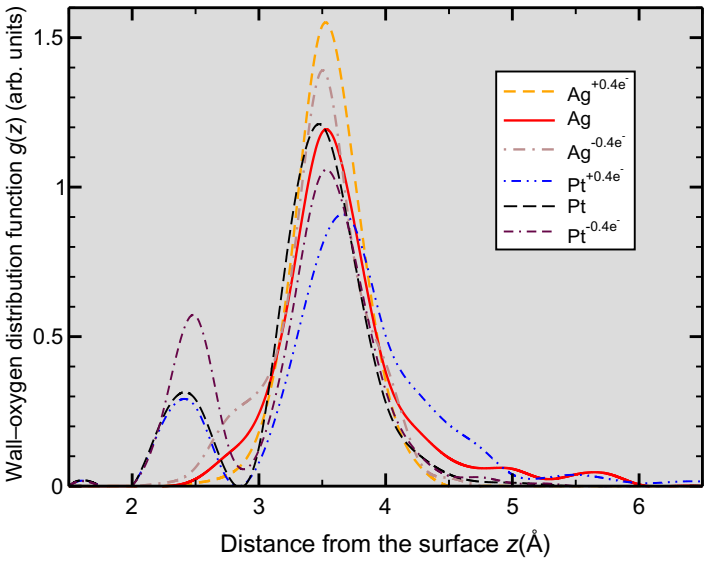

Figure 14. Wall–oxygen distribution function obtained from the AIMD simulations of the water at charged Ag(111) and Pt(111) substrates with 0.4 electrons added to the system ($+0.4e^-$) or subtracted from the system ($-0.4e^-$). In addition, the results for the uncharged substrates are shown.

be explained by the fact that the negatively charged oxygen atom is attracted by the positively charged Pt surface so that the water molecule in the parallel configuration becomes stabilized. However, the peak position hardly changes which simply means that the parallel configuration becomes more populated for a positively charged surface but that its distance from the surface remains almost unchanged. This is in agreement with previous DFT calculations considering a water bilayer at the Pd/Au(111) overlayer system which showed that applying an external electric field does not lead to any significant compression or expansion of the perfect water bilayer [22]. For the negatively charged surface, the first peak hardly changes at all, but the larger peak centered at 3.5 Å is shifted to slightly larger distances from the Pt(111) surface which can be understood considering the repulsion between the negatively charged substrate and the negatively charged oxygen atoms.

On Ag(111), we observe for the positively charged surface an additional shoulder of the main peak toward smaller distances to the surface, i.e. also here an attraction of the negatively charged oxygen atoms toward the surface occurs, but still no full second peak at smaller distances evolves. In the case of the negatively charged Ag(111) surface, the main peak becomes more narrow which does not seem to be consistent with the results for negatively charged Pt(111). In fact, we believe that this specific result is an artefact of our procedure to keep two of the oxygen atoms of the second layer vertically fixed to avoid the desorption of the water layer because we find that the water molecules become locked to these atoms in this particular case. This certainly deserves further investigations and simulations.

Finally, we address the vibrational spectrum of the water layers at the charged Pt(111) and Ag(111) surfaces which are plotted in figure 15. On both surfaces, the position and the width of the peaks for the OH bending and the O–H stretching vibrations did not change significantly with the charge which is in qualitative agreement with a recent SFG spectroscopy study of water

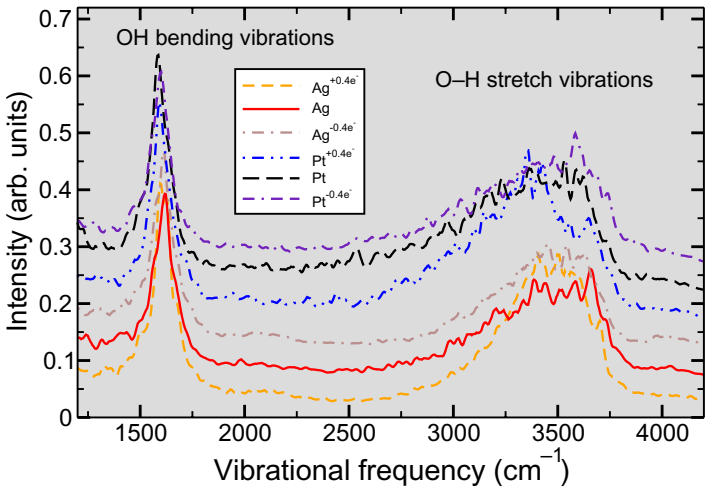

Figure 15. Vibrational spectrum of water bilayers on charged Ag(111) and Pt(111) surfaces obtained from the AIMD runs using the Fourier transform of the velocity–velocity autocorrelation function. The spectra have been averaged over ten different starting points.

layers on Au and Pt electrodes for varying electrode potentials [57]. Still interesting changes can be observed.

In particular, for both negatively charged surfaces there is a slight redshift of the O–H stretch vibrations. This seems to be surprising because for this charge state of the substrate the oxygen atoms of the water molecules are repelled from the surface. This is usually associated with a weaker interaction while a redshift of adsorbate vibrations is typically attributed to a stronger interaction. Obviously, the addition of charge to the metal–water interface weakens the O–H bonds. This seems to be a general effect since we found it both for the weakly interacting Ag(111) surface as well as for the more strongly interacting Pt(111) surface. Together with the findings for the vibrational spectra of water on the uncharged substrates (figure 9) this analysis shows that characteristic changes of vibrational spectra of water on metal surfaces are not necessarily due to different ordering behavior but that further aspects such as the orientation of the molecules and the charge present at the interface also influence the vibrational spectrum.

6. Conclusions

We have addressed the geometric and electronic structures of the metal–water interface by first-principles electronic structure calculations based on DFT. Ice-like hexagonal water bilayers on metal surfaces become strongly polarized which induces a work function reduction at the more strongly interacting transition metal surfaces, irrespective of the orientation of the bilayer. However, the polarization is basically restricted to the water bilayer, whereas the electronic structure of the metal substrate is only weakly influenced by the presence of the water layer.

According to AIMD simulations, the water bilayers become strongly distorted at room temperature. At the noble metal surfaces Ag(111) and Au(111), the hexagonal water structure is not stable and the water layer becomes disordered. The wall–oxygen distribution function of the first layer exhibits only one broad peak at distances that are much larger than the

equilibrium distance of an adsorbed water monomer from the surface. At the more strongly interacting transition metal surfaces Pt(111), Pd/Au(111) and Ru(0001), the simulations suggest that the hexagonal ordered structure might persist at room temperature, however, the orientation of the single water molecules is strongly fluctuating. Transitions between H-up and H-down configurations are well possible and occur frequently so that no distinction between an ordered H-up or an H-down structure can be made. This is also reflected in the work function changes induced by the thermalized water layers that lie between the corresponding values for ice-like H-up and H-down water bilayers. The stronger interaction also results in a redshift of the frequencies of the OH bending and the O–H stretch vibrations indicating the weakening of the water bonds.

Charging the metal substrates leads to small but characteristic changes. The change in the distance from the charged electrodes can be understood invoking electrostatics. The redshift of the O–H stretch vibrations at the negatively charged electrodes indicates that the addition of electronic charge to the metal–water interface weakens the intramolecular bonds. This also suggests that shifts in the vibrational spectra are not solely related to changes in the structure and order of the water bilayers.

Acknowledgments

This research was supported by the Konrad-Adenauer-Stiftung. Computer time on the BW-Grid of the federal state of Baden-Württemberg is gratefully acknowledged. Useful discussions with David Benoit, Wolfgang Schmickler and Eckhard Spohr are gratefully acknowledged.

References

[1] Thiel P A and Madey T E 1987 *Surf. Sci. Rep.* **7** 211
[2] Henderson M A 2002 *Surf. Sci. Rep.* **46** 1
[3] Verdaguer A, Sacha G M, Bluhm H and Salmeron M 2006 *Chem. Rev.* **106** 1478
[4] Izvekov S, Mazzolo A, Van Opdorp K and Voth G A 2001 *J. Chem. Phys.* **114** 3284
[5] Izvekov S and Voth G A 2001 *J. Chem. Phys.* **115** 7196
[6] Meng S, Xu L F, Wang E G and Gao S W 2002 *Phys. Rev. Lett.* **89** 176104
[7] Meng S, Wang E G and Gao S 2004 *Phys. Rev.* B **69** 195404
[8] Michaelides A, Alavi A and King D A 2004 *Phys. Rev.* B **69** 113404
[9] Michaelides A 2006 *Appl. Phys.* A **85** 415
[10] Toney M F, Howard J N, Richer J, Borges G L, Gordon J G, Melroy O R, Wiesler D G, Yee D and Sorensen L B 1994 *Nature* **368** 444
[11] Ito M 2008 *Surf. Sci. Rep.* **63** 329
[12] Feibelman P J 2002 *Science* **295** 99
[13] Spohr E 1989 *J. Phys. Chem.* **93** 6171
[14] Spohr E 1997 *J. Chem. Phys.* **107** 6342
[15] Raghavan K, Foster K, Motakabbir K and Berkowitz M 1991 *J. Chem. Phys.* **94** 2110
[16] Xia X and Berkowitz M L 1995 *Phys. Rev. Lett.* **74** 3193
[17] Siepmann J I and Sprik M 1995 *J. Chem. Phys.* **102** 511
[18] Crozier P S, Rowley R L and Henderson D 2000 *J. Chem. Phys.* **113** 9202
[19] Bukowski R, Szalewicz K, Groenenboom G C and van der Avoird A 2007 *Science* **315** 1249
[20] Santra B, Michaelides A, Fuchs M, Tkatchenko A, Filippi C and Scheffler M 2008 *J. Chem. Phys.* **129** 194111
[21] Lozovoi A Y, Alavi A, Kohanoff J and Lynden-Bell R M 2001 *J. Chem. Phys.* **115** 1661

[22] Roudgar A and Groß A 2005 *Chem. Phys. Lett.* **409** 157
[23] Filhol J S and Neurock M 2006 *Angew. Chem. Int. Ed. Engl.* **45** 402
[24] Taylor C D, Wasileski S A, Filhol J-S and Neurock M 2006 *Phys. Rev.* B **73** 165402
[25] Otani M and Sugino O 2006 *Phys. Rev.* B **73** 115407
[26] Skúlason E, Karlberg G S, Rossmeisl J, Bligaard T, Greeley J, Jónsson H and Nørskov J K 2007 *Phys. Chem. Chem. Phys.* **9** 3241
[27] Zhao J, Chan C T and Che J G 2007 *Phys. Rev.* B **75** 085435
[28] Sugino O, Hamada I, Otani M, Morikawa Y, Ikeshoji T and Okamoto Y 2007 *Surf. Sci.* **601** 5237
[29] Otani M, Hamada I, Sugino O, Morikawa Y, Okamoto Y and Ikeshoji T 2008 *Phys. Chem. Chem. Phys.* **10** 3609
[30] Gohda Y, Schnur S and Groß A 2009 *Faraday Discuss.* **140** 233
[31] Filhol J S and Bocquet M-L 2007 *Chem. Phys. Lett.* **438** 203
[32] Kresse G and Furthmüller J 1996 *Phys. Rev.* B **54** 11169
[33] Perdew J P, Burke K and Ernzerhof M 1996 *Phys. Rev. Lett.* **77** 3865
[34] Vassilev P, Hartnig C, Koper M T M, Frechard F and van Santen R A 2001 *J. Chem. Phys.* **115** 9815
[35] VandeVondele J, Mohamed F, Krack M, Hutter J, Sprik M and Parrinello M 2005 *J. Chem. Phys.* **122** 014515
[36] Blöchl P E 1994 *Phys. Rev.* B **50** 17953
[37] Kresse G and Joubert D 1999 *Phys. Rev.* B **59** 1758
[38] Vassilev P, van Santen R A and Koper M T M 2005 *J. Chem. Phys.* **122** 054701
[39] Materzanini G, Tantardini G F, Lindan P J D and Saalfrank P 2005 *Phys. Rev.* B **71** 155414
[40] Menzel D 2002 *Science* **295** 58
[41] Heras J M and Viscido L 1980 *Appl. Surf. Sci.* **4** 238
[42] Roudgar A and Groß A 2003 *Phys. Rev.* B **67** 033409
[43] Roudgar A and Groß A 2003 *J. Electroanal. Chem.* **548** 121
[44] Groß A 2006 *Top. Catal.* **37** 29
[45] Prada S, Martinez U and Pacchioni G 2008 *Phys. Rev.* B **78** 235423
[46] Roudgar A and Groß A 2005 *Surf. Sci.* **597** 42
[47] Langenbach E, Spitzer A and Lüth H 1984 *Surf. Sci.* **147** 179
[48] Kiskinova M, Pirug G and Bonzel H 1985 *Surf. Sci.* **150** 319
[49] Hoffmann W and Benndorf C 1997 *Surf. Sci.* **377–379** 681
[50] Lilach Y, Romm L, Livneh T and Asscher M 2001 *J. Phys. Chem.* B **105** 2736
[51] Groß A 2002 *Surf. Sci.* **500** 347
[52] Daw M S and Baskes M I 1984 *Phys. Rev.* B **29** 6443
[53] Vassilev P, Koper M T M and van Santen R A 2002 *Chem. Phys. Lett.* **359** 337
[54] Hartnig C and Spohr E 2005 *Chem. Phys.* **319** 185
[55] Jacobi K, Bedürftig K, Wang Y and Ertl G 2001 *Surf. Sci.* **472** 9
[56] Groß A and Dianat A 2007 *Phys. Rev. Lett.* **98** 206107
[57] Noguchi H, Okada T and Uosaki K 2009 *Faraday Discuss.* **140** 125
[58] Osawa M, Tsushima M, Mogami H, Samjeske G and Yamakata A 2008 *J. Phys. Chem.* C **112** 4248
[59] Ye S, Nihonyanagi S and Uosaki K 2001 *Phys. Chem. Chem. Phys.* **3** 3463
[60] Schmitz M and Tavan P 2004 *J. Chem. Phys.* **121** 12247
[61] Ibach H and Lehwald S 1980 *Surf. Sci.* **91** 187
[62] Thiel P A, DePaola R A and Hoffmann F M 1984 *J. Chem. Phys.* **80** 5326
[63] Ogasawara H, Yoshinobu J and Kawai M 1999 *J. Chem. Phys.* **111** 7003
[64] Feibelman P J 2003 *Phys. Rev.* B **67** 035420
[65] Xu L, Xiao H and Zu X 2005 *Chem. Phys.* **315** 155
[66] Clay C, Haq S and Hodgson A 2004 *Chem. Phys. Lett.* **388** 89
[67] Tatarkhanov M, Fomin E, Salmeron M, Andersson K, Ogasawara H, Pettersson L G M, Nilsson A and Cerdá J I 2008 *J. Chem. Phys.* **129** 154109

[68] Schmickler W 1996 *Chem. Rev.* **96** 3177
[69] Neugebauer J and Scheffler M 1992 *Phys. Rev.* B **46** 16067
[70] Toney M F, Howard J N, Richer J, Borges G L, Gordon J G, Melroy O R, Wiesler D G, Yee D and Sorensen L B 1995 *Surf. Sci.* **335** 326
[71] Morgenstern K and Nieminen J 2004 *J. Chem. Phys.* **120** 10786
[72] Fu C L and Ho K M 1989 *Phys. Rev. Lett.* **63** 1617
[73] Bohnen K P and Kolb D M 1998 *Surf. Sci.* **407** L629
[74] Lozovoi A Y and Alavi A 2003 *Phys. Rev.* B **68** 245416
[75] Che J G and Chan C T 2003 *Phys. Rev.* B **67** 125411
[76] Wasileski S A and Janik M J 2008 *Phys. Chem. Chem. Phys.* **10** 3613
[77] Rossmeisl J, Skúlason E, Björketun M J, Tripkovic V and Nørskov J K 2008 *Chem. Phys. Lett.* **466** 68